Empirical Site Classification of CSN Network Using Strong-Motion Records

by F. Leyton, C. Pastén, S. Ruiz, B. Idini, and F. Rojas

ABSTRACT

The National Seismological Center of the University of Chile (CSN, Centro Sismológico Nacional) has been operating more than 400 seismic stations throughout the country. The data collected from this network, from March 2012 to August 2017, includes more than 4000 Chilean strong-motion records, from more than 1000 events (magnitudes ranging from 4.0 up to 8.3). In this study, we use this data set and classify 118 stations from this network, using the horizontal-to-vertical response spectral ratio (HVRSR) of strong-motion records. This classification considers not only the predominant period obtained from the average HVRSR but also the peak amplitude from this curve. The results indicate no correlation between the two parameters, despite the common practice of combining all curves with similar predominant periods. Even more, we believe that relevant information of the site's impedance contrast between the soil and bedrock is lost in the process of averaging HVRSR curves from different stations.

Electronic Supplement: Figure showing an example of the combination of two horizontal-to-vertical response spectral ratio (HVRSR) from stations with the same classification, and table with details of the location, the number of records used in the computation of the HVRSR, and the classification using the predominant period and the unique peak of the HVRSR.

INTRODUCTION

The National Seismological Center of the University of Chile (CSN, Centro Sismológico Nacional) has been operating more than 100 multiparametric stations, composed of broadband seismometers, accelerometers, and Global Navigation Satellite Systems instruments, as well as nearly 300 strong-motion stations (Barrientos, 2018; Leyton *et al.*, 2018). This network has been recording a large amount of strong-motion data, including the 2014 Iquique earthquake (M_w 8.2), the 2015 Illapel earthquake (M_w 8.3), and the 2016 Chiloé earthquake (M_w 7.6), along with its corresponding aftershocks (for details, see Ruiz *et al.*, 2014, 2016, 2017, respectively) and several moderate magnitude events (Fig. 1). These strong-motion records are periodically incorporated to the CSN's Strong-Motion Database (SMDB; see Data and Resources for details). In average, the SMDB incorporates 33 new strong-motion records of events from magnitude 4.0 and up every month, without considering the occurrence of major earthquakes and their corresponding aftershocks. From March 2012 to August 2017, this database included more than 4000 Chilean strong-motion records of more than 1000 events, whose magnitudes ranged between 4.0 and 8.3 (see Fig. 1). The network's stations are located in a variety of soils types, ranging from hard rock (average S-wave velocity in the upper 30 m: $V_{S30} > 1500$ m/s) to soft soils ($V_{S30} < 300$ m/s) (Leyton *et al.*, 2018). To improve our understanding of these strong-motion records, we need to gain knowledge of the dynamic behavior by this variety of site conditions.

Local site conditions play a key role in the signals recorded during earthquakes (e.g., Borcherdt, 1970; Anderson *et al.*, 1996). The knowledge of these characteristics is essential to understand the shaking produced by large events (Shearer and Orcutt, 1987), causing amplifications in different period ranges of the response spectrum during an event (Mohraz, 1976; Seed *et al.*, 1976; Lachet *et al.*, 1996). In this sense, the main objective of a successful site classification is to aggregate a set of sites into previously defined classes, so that the strong-motion records in a given site class present similar characteristics such as site amplification and predominant vibration periods. The pioneer work by Seed *et al.* (1976), using the normalized shape of strong-motion response spectra (with a 5% damping ratio), clearly showed the relevance of site conditions on the overall spectral shapes. Later on, the use of the V_{S30} as a proxy for site classification gained relevance in many engineering standard codes and empirical ground motion prediction equations (GMPEs) due to the simplicity estimating it with invasive and noninvasive geophysical methods. However, limitations in the prediction of seismic amplification, especially in sites with deeper sediments (Castellaro *et al.*, 2008; Lee and Trifunac, 2010), required the introduction of additional variables such as the site predominant period. In fact, Yamazaki and Ansary (1997) presented evidence of the effects of hypocentral distance, magnitude, and depth on a set of over 2000 Japanese ground motions. To remove these effects, these authors proposed the use of horizontal-to-vertical (H/V) Fourier spectrum

 doi: 10.1785/0220170167

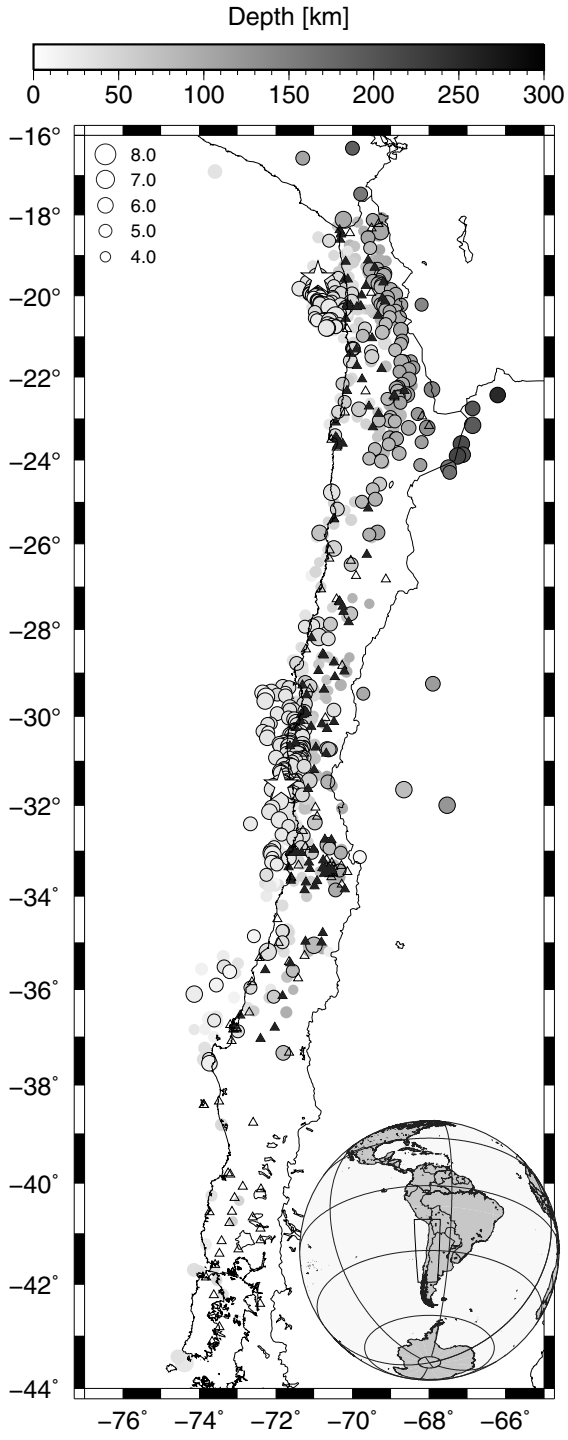

▲ **Figure 1.** Location of the 1086 events (circles) and the 246 stations (triangles) from the Centro Sismológico Nacional Strong-Motion Database; the insert shows the study region in South America. For the events (circles), the gray scale is proportional to the depth (following the scale on the top) whereas the size is proportional to the magnitude (following the scale in the upper left corner). The events (circles) and stations (triangles) used in this study are surrounded by a thin black line and filled in black, respectively. White stars show the hypocenter of the two large interplate earthquakes: Iquique 2014 (M_w 8.2) and Illapel 2015 (M_w 8.3) earthquakes, from top to bottom, respectively.

ratios from the strong-motion data, enabling a site classification. Lermo and Chávez-García (1993) proposed that, for sites with simple geology, the H/V spectral ratio of strong-motion records could be used to estimate the predominant period and the local amplification level. Later on, Zare *et al.* (1999) succeeded in performing a site classification for a set of Iranian stations using these H/V spectral ratios, in addition to V_{S30}. Based on these results, recent studies used this information to verify previous classifications developed with traditional methods (Lee *et al.*, 2001; Ghasemi *et al.*, 2009). Furthermore, some studies relied on the H/V spectral ratio to classify or complement other parameters used for soil classification (Luzi *et al.*, 2011; Castellaro and Mulargia, 2014). These methodologies were also supported by results showing that the predictive capabilities of the predominant period were comparable to V_S-based parameters and, in some cases, it performed even better (Zhao and Xu, 2013; Ghofrani and Atkinson, 2014). A disadvantage of the classification based on the predominant period is that high dispersion in amplification can be found in sites characterized with a similar predominant period (Di Alessandro *et al.*, 2012). In addition, some sites may present multiple peak periods and broadband amplification, none of which can be directly related to site amplification during earthquakes.

Recently, Zhao *et al.* (2006) and Idini *et al.* (2017) proposed GMPEs for subduction environments using the horizontal-to-vertical response spectral ratio (HVRSR) to provide the site classification. Furthermore, several authors have shown that the HVRSR adequately provides the site's seismic signature (Fukushima *et al.*, 2007; Di Alessandro *et al.*, 2012; Zhao and Xu, 2013). They considered the predominant period ($T*$) of a site as the period in which the average HVRSR has a unique peak value ($P*$), defining categories from s_{II} to s_V (see Table 1 for details). Sites with HVRSR amplitudes consistently lower than 2 were classified as a reference rock site s_I; on the other hand, sites with a broadband of amplification or multiple peaks, were classified as s_{VI}, as done by Di Alessandro *et al.* (2012) (see Table 1 for details). For sites with a unique predominant peak (classes s_{II}–s_V), Idini *et al.* (2017) observed large standard deviations in the resulting averaged amplitudes; hence, they included an additional parameter $P*$ in their classification, as shown in Table 1 (examples of this classification are presented in Fig. 2). Considering both $T*$ and $P*$, we present the classification of 118 strong-motion stations, out of 246 stations that have recorded strong-motion accelerograms, present at the SMDB (see Fig. 1 and Ⓔ Table S1, available in the electronic supplement to this article).

METHODOLOGY

We considered records from events with magnitudes larger or equal to 5.0 and hypocentral distances smaller than 500 km (Fig. 1), following the criteria adopted by Idini *et al.* (2017). All these records were obtained from the Chilean SMDB, managed by the CSN (see Data and Resources for details). For the present study, 373 events with magnitudes larger or equal to 5.0

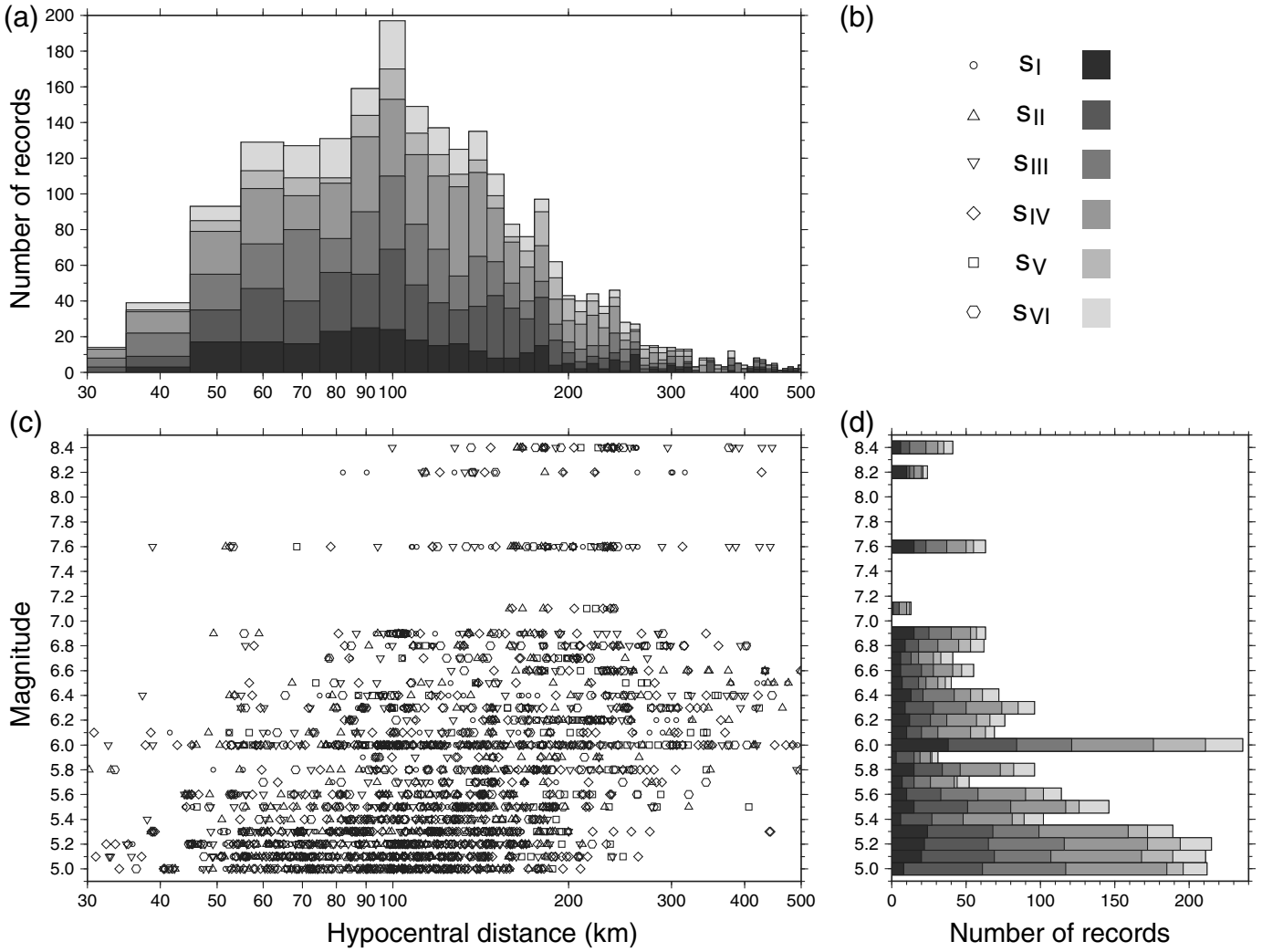

▲ **Figure 2.** (c) Distribution of records as a function of magnitude, hypocentral distance, and classification according to the predominant period, following the legend on (b). (a,d) The histograms of records as a function of (a) hypocentral distance and (d) magnitude. For these panels, the shades of grays represent a different class, following the legend on (b).

were considered (see Fig. 1). We include two events with magnitudes larger than 8.0: the 2014 Iquique (M_w 8.1) and the 2015 Illapel (M_w 8.3) earthquakes (white stars in Fig. 1), and their corresponding aftershocks. From all the events, 59% corresponds to interplate thrust earthquakes and 41% to intermediate depth intraslab earthquakes. From these events, we compiled a total of 2319 records, gathered at hypocentral distances ranging from 30 up to 500 km. A disaggregate analysis of the records is presented in Figure 2, along with the corresponding histograms with respect to hypocentral distance and magnitude. Figure 2 shows no bias for a specific site class with respect to event magnitude or hypocentral distance: all site classes have a clear contribution of diverse set of event magnitudes and hypocentral distances. Nevertheless, histograms in Figure 2 show that most of the records have a hypocentral distance of 100 km (nearly 200 records), whereas almost 240 records belong to events of magnitude 6.0. From this data set, we did not find significant evidence of variations in the site response between moderate and large magnitude events.

For each record, we proceeded as follows: we removed the linear trend and computed the response spectrum (with a 5% damping ratio) for 100, logarithmically spaced, periods from 0.1 to 10 s. The total horizontal response spectrum was computed by the arithmetic average of the two horizontal components, to be subsequently divided, period by period by the vertical spectra; thus obtaining the HVRSR. We successfully classify a station if we had more than five records and, exceptionally, after detailed examination, with only four records; stations with less than four records were not considered. Finally, we computed the arithmetic average and standard deviation as a function of period, for every station. From a total of 246 stations with available strong-motion records, only 118 fulfilled the preceding requirements, enabling their classification.

From the resulting average HVRSR, we classify each station following Idini *et al.* (2017): first, we determined the predominant period ($T*$) of the station as the period where the average HVRSR shows a unique peak, with amplitude larger than 2. From this value, we classify the station following

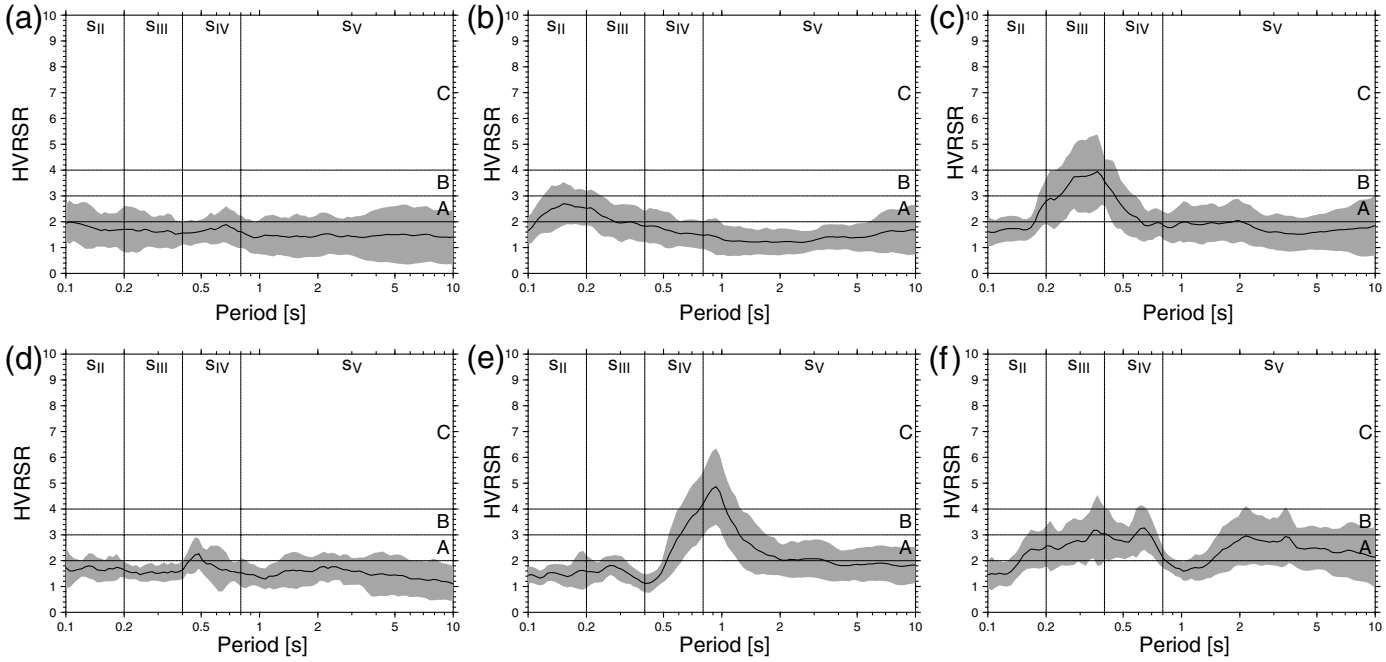

▲ **Figure 3.** Examples of the resulting average horizontal-to-vertical response spectral ratio (HVRSR) for the following stations: (a) T09A, (b) C10O, (c) C33O, (d) R14M, (e) C20O, and (f) PB11. Also, the shown examples of the categories used following the predominant period ($T*$) and the HVRSR unique peak amplitude ($P*$): (a) s_I, (b) $s_{II}A$, (c) $s_{III}B$, (d) $s_{IV}A$, (e) s_VC, and (f) s_{VI}. Thin dashed lines represent the limits of the used classifications: vertical for $T*$ and horizontal for $P*$.

the limits shown in Table 1. Second, we determined the amplitude of the unique peak of the average HVRSR ($P*$) and, only for those cases were $P*$ exceeds 2, this value was used for the additional classification, as presented in Table 1. Figure 3 presents some examples of the resulting average HVRSR (continuous line) and its corresponding standard deviation (gray area); see figure caption for details. In Figure 3, we present an example of each class of $T*$: (a) s_I, (b) s_{II}, (c) s_{III}, (d) s_{IV}, (e) s_V, and (f) s_{VI}. For all panels, both classifications ($T*$ and $P*$) are shown in thin dashed lines and labeled at the top (for $T*$) and the right (for $P*$).

Table 1
Site Classification Used in This Study (Proposed by Idini *et al.*, 2017), Based Average Horizontal-to-Vertical Response Spectral Ratio (HVRSR)

Site Classification	
Classes for $T*$	**$T*$ (s)**
s_I	—
s_{II}	$T* \le 0.2$
s_{III}	$0.2 < T* \le 0.4$
s_{IV}	$0.4 < T* \le 0.8$
s_V	$T* > 0.8$
s_{VI}	Not identifiable or BB amplification or 2+ peaks
Classes for $P*$	**$P*$**
A	$2 \le P* < 3$
B	$3 \le P* < 4$
C	$P* \ge 4$

Classifications based on the site predominant period ($T*$) and the unique peak amplitude ($P*$).

RESULTS

Figure 4 presents the classification of the 118 strong-motion stations considering predominant period ($T*$) and HVRSR unique peak amplitude ($P*$). Figure 4 shows no clear correlation between the location of the station and its classification, using neither $T*$ nor $P*$.

Figure 5 presents a summary of the results, as a function of the predominant period ($T*$) and the HVRSR unique peak value ($P*$), for all those sites with one clear peak (i.e., sites with classes s_{II}–s_V). We also added a simple classification of rock or soil condition based on surface geology, obtained from the National Geological Map (Sernageomin, 2004), shown in Ⓔ Table S1. From these results, we estimated the percentage of sites, within each class, that correspond to rock and soil, shown in Ⓔ Table S2. For example, for class s_I, 83% of the sites correspond to rock, while for sites with long periods (classes s_{III}, s_{IV}, and s_V, with $T* > 0.2$ s), at least 80% of the sites correspond to soils; on the other hand, for class s_{II}, characterized by short periods ($T* < 0.2$ s), there is a mixture between soils (55%) and rock (45%). Finally, sites with a broadband of amplification or multiple peaks (class s_{VI}), we found a

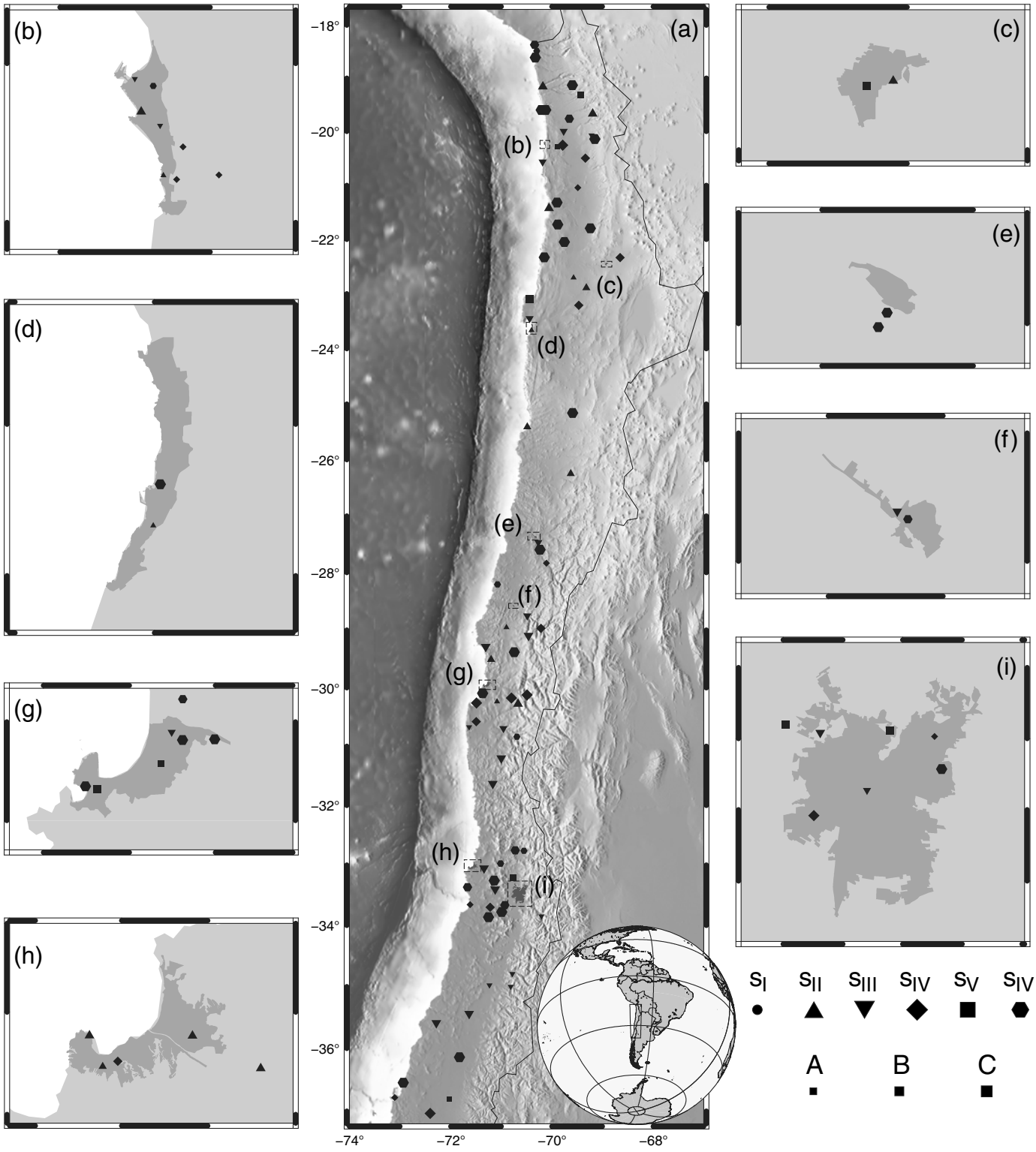

▲ **Figure 4.** (a) The location of the stations classified in this study: each symbol represents a classification following the predominant period ($T*$), using the definition shown at the lower-right corner; the inset shows the study region in South America. The size is proportional to the classification considering the peak HVRSR amplitude ($P*$) following the definition at the lower-right corner. Each subpanel presents a zoom to a city: (b) Iquique, (c) Calama, (d) Antofagasta, (e) Copiapó, (f) Vallenar, (g) La Serena and Coquimbo, (h) Valparaíso and Viña del Mar, and (i) Santiago.

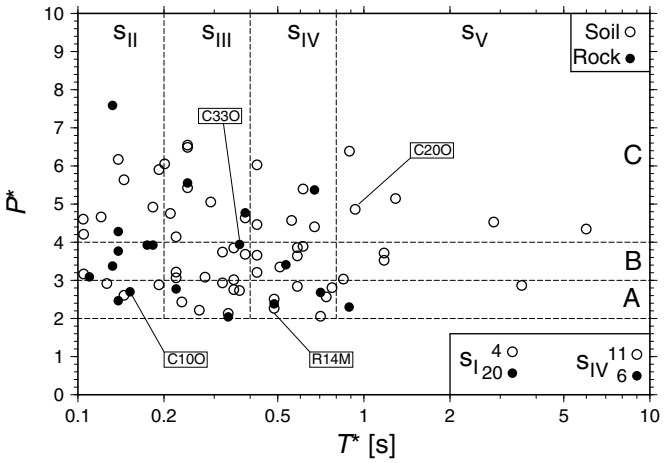

▲ **Figure 5.** Each dot represents a site's HVRSR peak amplitude ($P*$) and predominant period ($T*$) pair, for all sites with a single, clear, peak; that is, classes s_{II}–s_V. Filled and empty circles represent rock and soil conditions, based on surface geology (see top legend); results for classes' s_I and s_{VI} are presented in the bottom legend. Dashed lines mark the limits in period (vertical lines) and amplitude (horizontal lines); labels on top and right side follow the classification shown in Table 1. Labels mark the stations presented in Figure 2.

slight predominance of soils (65%) over rock sites (35%). It is worth noting that the geologic surface classification comes from a 1:1,000,000 map; hence, we would expect possible errors in this classification. Additionally, Figure 5 shows no evident correlation between the site's $T*$ and its corresponding $P*$; furthermore, we computed the Pearson correlation coefficient (r) between both variables and obtained $r = 0.13$. Hence, these parameters are completely independent and quantify different characteristics at a given site.

Previous studies have not considered $P*$ as a parameter in their classification (Zhao *et al.*, 2006; Fukushima *et al.*, 2007; Di Alessandro *et al.*, 2012; Zhao and Xu, 2013). Even more, Ghofrani and Atkinson (2014) proposed a relationship between $T*$ and $P*$ (see equation 9a from their work). However, from figure 7 of Ghofrani and Atkinson (2014), we see a large variability in $P*$, ranging from 2.5 up to 4.0, also observed by Idini *et al.* (2017). We believe that this variability is the result of combining sites with different dynamic properties in the same site class such as the impedance contrast between the soil and bedrock, as discussed by several authors (e.g., Ghofrani *et al.*, 2013; Castellaro and Mulargia, 2014). Hence, these variations will lead to errors in the potential amplification of any given site (Idini *et al.*, 2017). To test this hypothesis, we computed the average HVRSR for two stations with the same $T*$ classification, as shown in Ⓔ Figure S1. Ⓔ Figure S1 shows that T07A (red) presents a large $P*$-value, whereas R14M (green) is barely over 2; however, the average (shown in dashed black line) lies in between, probably loosing relevant information of the each site's impedance contrast.

We tested this classification performance by computing the root mean square (rms) between the observed response spectra and the predicted by the GMPE defined by Idini *et al.* (2017), considering the results found in this study. We obtained an rms of 0.577 ± 0.332; the results for all stations are shown in Ⓔ Table S1. These results validate the used classification based on HVRSR, considering predominant period $T*$ and peak amplitude $P*$ as a key parameters.

FINAL COMMENTS

The CSN network (operating since 2012) has been continuously collecting strong-motion records from moderate-to-large magnitude Chilean earthquakes; however, the lack of information regarding the dynamic behavior of the sites limits its usability. In the present study, we applied the empirical site classification proposed by Idini *et al.* (2017) to this network and were able to classify 118 strong-motion stations. This classification is based on the results of the average HVRSR, considering both its predominant period ($T*$) and unique peak amplitude ($P*$). Using a simple, geologic-based, classification between rock and soil site conditions, we found clear agreement with the results obtained here, despite the fact of being based in a 1:1,000,000 National Geologic Map. Furthermore, we tested the classification performance comparing the observed response spectra and the predicted by Idini *et al.* (2017) using the values shown in Ⓔ Table S1, finding an rms of 0.577 ± 0.332, validating our results.

On the other hand, from the results obtained here, no correlation is found between $T*$ and $P*$; even more, the process of averaging HVRSR curves from different stations produces the loss of relevant information of the site's impedance contrast between the soil and bedrock. Hence, we believe that both parameters are required for a complete description of amplification and meaningful site classification.

DATA AND RESOURCES

All the data used in this study is freely available in the Chilean Strong-Motion Database (SMDB), maintained by the Centro Sismológico Nacional (CSN; evtdb.csn.uchile.cl, last accessed August 2017).

ACKNOWLEDGMENTS

The authors thank two anonymous reviewers and the guest editor for their valuable comments that greatly improved this article. The authors acknowledge the support of FONDECYT N° 1170430 to this study. Figures were made using Generic Mapping Tool (GMT) software (Wessel and Smith, 1998).

REFERENCES

Anderson, J. G., Y. Lee, Y. Zeng, and S. Day (1996). Control of strong motion by the upper 30 m, *Bull. Seismol. Soc. Am.* **86,** 1749–1759.

Barrientos, S. (2018). The new Chilean seismic network, *Seismol. Res. Lett.* doi: 10.1785/0220160195.

Borcherdt, R. D. (1970). Effects of local geology on ground motion near San Francisco Bay, *Bull. Seismol. Soc. Am.* **60,** 29–61.

Castellaro, S., and F. Mulargia (2014). Simplified seismic soil classification: The Vfz matrix, *Bull. Earthq. Eng.* **12,** no. 2, 735–754.
Castellaro, S., F. Mulargia, and P. L. Rossi (2008). V_{S30}: Proxy for seismic amplification? *Seismol. Res. Lett.* **79,** no. 4, 540–543.
Di Alessandro, C., L. F. Bonilla, D. M. Boore, A. Rovelli, and O. Scotti (2012). Predominant-period site classification for response spectra prediction equations in Italy, *Bull. Seismol. Soc. Am.* **102,** no. 2, 680–695.
Fukushima, Y., L. F. Bonilla, O. Scotti, and J. Douglas (2007). Site classification using horizontal-to-vertical response spectral ratios and its impact when deriving empirical ground-motion prediction equations, *J. Earthq. Eng.* **11,** no. 5, 712–724.
Ghasemi, H., M. Zare, Y. Fukushima, and F. Sinaeian (2009). Applying empirical methods in site classification, using response spectral ratio (H/V): A case study on Iranian strong motion network (ISMN), *Soil Dynam. Earthq. Eng.* **29,** no. 1, 121–132.
Ghofrani, H., and G. M. Atkinson (2014). Site condition evaluation using horizontal-to-vertical response spectral ratios of earthquakes in the NGA-West 2 and Japanese databases, *Soil Dynam. Earthq. Eng.* **67,** 30–43.
Ghofrani, H., G. M. Atkinson, and K. Goda (2013). Implications of the 2011 M9.0 Tohoku Japan earthquake for the treatment of site effects in large earthquakes, *Bull. Earthq. Eng.* **11,** no. 1, 171–203.
Idini, B., F. Rojas, S. Ruiz, and C. Pastén (2017). Ground motion prediction equations for the Chilean subduction zone, *Bull. Earthq. Eng.* **15,** no. 5, 1853–1880, doi: 10.1007/s10518-016-0050-1.
Lachet, C., D. Hatzfeld, P.-Y. Bard, N. Theodulidis, C. Papaioannou, and A. Savvaidis (1996). Site effects and microzonation in the city of Thessaloniki (Greece) comparison of different approaches, *Bull. Seismol. Soc. Am.* **86,** 1692–1703.
Lee, C.-T., C.-T. Cheng, C.-W. Liao, and Y.-B. Tsai (2001) Site classification of Taiwan free-field strong-motion stations, *Bull. Seismol. Soc. Am.* **91,** 1283–1297.
Lee, V. W., and M. D. Trifunac (2010). Should average shear-wave velocity in the top 30m of soil be used to describe seismic amplification? *Soil Dynam. Earthq. Eng.* **30,** no. 11, 1250–1258.
Lermo, J., and F. J. Chávez-García (1993). Site effect evaluation using spectral ratios with only one station, *Bull. Seismol. Soc. Am.* **83,** 1574–1594.
Leyton, F., A. Leopold, G. Hurtado, C. Pastén, S. Ruiz, G. Montalva, and E. Saéz (2018). Geophysical characterization of the Chilean seismological stations: First results, *Seismol. Res. Lett.* doi: 10.1785/0220170156 (this issue).
Luzi, L., R. Puglia, F. Pacor, M. R. Gallipoli, D. Bindi, and M. Mucciarelli (2011). Proposal for a soil classification based on parameters alternative or complementary to $V_{S,30}$, *Bull. Earthq. Eng.* **9,** no. 6, 1877–1898.
Mohraz, B. (1976). A study of earthquake response spectra for different geological conditions, *Bull. Seismol. Soc. Am.* **66,** 915–935.
Ruiz, S., E. Klein, F. del Campo, E. Rivera, P. Poli, M. Metois, V. Christophe, J. C. Baez, G. Vargas, F. Leyton, and R. Madariaga (2016). The seismic sequence of the 16 September 2015 M_w 8.3 Illapel, Chile, earthquake, *Seismol. Res. Lett.* **87,** no. 4, 789–799, doi: 10.1785/0220150281.
Ruiz, S., M. Metois, A. Fuenzalida, J. Ruiz, F. Leyton, R. Grandin, C. Vigny, R. Madariaga, and J. Campos (2014). Intense foreshocks and a slow slip event preceded the 2014 Iquique M_w 8.1 earthquake, *Science* **345,** no. 6201, 1165–1169.
Ruiz, S., M. Moreno, D. Melnick, F. del Campo, P. Poli, J. C. Baez, F. Leyton, and R. Madariaga (2017). Reawakening of large earthquakes in South-Central Chile: The 2016 M_w 7.6 Chiloé event, *Geophys. Res. Lett.* **44,** no. 13, 6633–6640, doi: 10.1002/2017GL074133.
Seed, H. B., C. Ugas, and J. Lysmer (1976). Site-dependent spectra for earthquake-resistant design, *Bull. Seismol. Soc. Am.* **66,** 221–243.
Sernageomin (2004). Mapa Geológico de Chile: versión digital, *Servicio Nacional de Geología y Minería, Publicación Geológica Digital*, No. 7 (CD-ROM, versión 1.0, 2004), Santiago, Chile (in Spanish).
Shearer, P. M., and J. A. Orcutt (1987). Surface and near-surface effects on seismic waves theory and borehole seismometer results, *Bull. Seismol. Soc. Am.* **77,** 1168–1196.
Wessel, P., and W. H. F. Smith (1998). New improved version of generic mapping tools released, *Eos Trans. AGU* **79,** 579.
Yamazaki, F., and M. A. Ansary (1997). Horizontal-to-vertical spectrum ratio of earthquake ground motion for site characterization, *Earthq. Eng. Struct. Dynam.* **26,** 671–689.
Zare, M., P. Y. Bard, and M. Ghafory-Ashtiany (1999). Site characterizations for the Iranian strong motion network, *Soil Dynam. Earthq. Eng.* **18,** no. 2, 101–123.
Zhao, J. X., and H. Xu (2013). A comparison of V_{S30} and site period as site-effect parameters in response spectral ground-motion prediction equations, *Bull. Seismol. Soc. Am.* **103,** no. 1, 1–18.
Zhao, J. X., J. Zhang, A. Asano, Y. Ohno, T. Oouchi, T. Takahashi, H. Ogawa, K. Irikura, H. K. Thio, P. G. Somerville, *et al.* (2006). Attenuation relations of strong ground motion in Japan using site classification based on predominant period, *Bull. Seismol. Soc. Am.* **96,** 898–913.

F. Leyton
Centro Sismológico Nacional
Universidad de Chile
Blanco Encalada 2002
Santiago, Chile
leyton@csn.uchile.cl

C. Pastén
Department of Civil Engineering
Universidad de Chile
Blanco Encalada 2002
Santiago, Chile
cpasten@ing.uchile.cl

S. Ruiz
Department of Geophysics
Universidad de Chile
Blanco Encalada 2002
Santiago, Chile
sruiz@dgf.uchile.cl

B. Idini
Seismological Laboratory
California Institute of Technology
1200 E. California Boulevard
South Mudd Building, Room 360, MS 252-21
Pasadena, California 91125 U.S.A.
bidini@ing.uchile.cl

F. Rojas
Department of Civil Engineering
Universidad de Chile
Blanco Encalada 2002
Santiago, Chile
fabianrojas@uchile.cl

Published Online 14 February 2018